6

X-RAY EMISSION TECHNIQUES

6.0 INTRODUCTION

Three techniques involving the use of X-ray emission to obtain quantitative elemental analysis of materials are described in this chapter. They are X-Ray Fluorescence, XRF, Total Reflection X-Ray Fluorescence, TXRF, and Particle-Induced X-Ray Emission, PIXE. XRF and TXRF use laboratory X-ray tubes to excite the emission. PIXE uses high-energy ions from a particle accelerator.

The X-ray emission process following the excitation is the same in all three cases, as it is also for the electron-induced X-ray emission methods (EDS and EMPA) described in Chapter 3. The electron core hole produced by the excitation is filled by an electron falling from a shallower level, the excess energy produced being released as an emitted X ray with a wavelength characteristic of the atomic energy levels involved. Thus elemental identification is provided and quantification can be obtained from intensities. The practical differences between the techniques come from the consequences of using the different excitation sources.

In XRF all elements having $Z > 3$ can be detected using WDS (see Chapter 3), though a range of excitation tubes and analyzing crystal monochromators is needed. If EDS (see Chapter 3) is used spectral resolution is much poorer, resulting in overlapping peaks and a reduced ability to distinguish some elements at low concentrations. Also only $Z > 10$ can usually be detected. The sample is examined in air, usually with an unfocused X-ray beam without lateral resolution, though special microbeam systems down to 10 μm do exist. For normal usage X-ray penetration will be many microns, resulting in essentially bulk analysis. With special equipment angles of incidence close to grazing can be used, reducing the probing depth considerably (down to 1000 Å). Large-area flat samples are then needed.

Atomic detection limits are around 0.1% for $Z > 15$ with a few percent accuracy. Detection limits for light elements are much poorer since they go roughly as Z^2. The quantification algorithms account for several correct ion factors. XRF has been widely used for solids, powders, and liquids, and more recently for simultaneous determination of both composition and thickness of single and multilayer thin films in the range of a few hundred angstroms to several microns. Such determinations are computer iterative fits to assumed models, however, and so are not necessarily unique.

In TXRF the angle of incidence of excitation is reduced to a few mrad. which is below the total reflection angle. Only a few tens of angstroms contribute to the signal under these conditions. The X-ray optics conditions are stringent for this approach, however, and very flat, large-area samples are needed. The method is therefore readily tailored to Si and GaAs wafers, where it is becoming widely used to monitor homogeneous surface impurities at concentrations down to 10^{10}–10^{11} atoms/cm^2 for heavy metals and 10^{12}–10^{13} atoms/cm^2 for elements such as Si, S, and Cl on GaAs. The method is also useful for thin-film interfaces and multilayers. A variation of the technique is vapor phase decomposition, VPD, where the surface of a Si wafer is dissolved in HF. The resulting solution of impurities is evaporated in the center of the wafer which is then analyzed by TXRF. The sensitivity can be improved two to three orders of magnitude this way. The cost of TXRF can be up to $600,000 compared to the more modest $50,000 to $300,000 for XRF.

PIXE is an adjunct to RBS (see Chapter 9), using the same particle beam (H or He ions usually) and the same analysis chamber with an added EDS detector. Probing depths for a 2–4-MeV beam (the usual energies) are microns, similar to XRF, but control is possible by going to higher or lower energies. Often there is no lateral resolution but microbeam systems down to a few microns spot size do exist. PIXE tends to be used more for surface layer and thin-film analysis than for bulk samples. Its major use has been in the biomedical area, where it has some advantages over XRF in the microbeam mode. Insulators can be a problem because of build up of high charges, leading to discharges. PIXE's strength should be its complementary nature to RBS, since it provides unambiguous identification for some elements that are hard to separate by RBS; it is more sensitive to low-Z elements in high-Z materials; and it is better at trace analysis in general. RBS, on the other hand, provides a quantitative depth profile of the major constituents, provided they are resolvable. Altogether, however, PIXE usage is only about 1% that of XRF.

One should compare capabilities to the electron beam X-ray emission methods of Chapter 3. The major difference is the higher lateral resolution with electron beams and the associated mapping capabilities. Another difference is the shorter probing depth possible with electrons, except when compared to the specialized TXRF method. Comparing electron-beam EDS to X-ray/particle EDS or electron-beam WDS to X-ray/particle WDS, the electron beams have poorer detection limits because of the greater X-ray background associated with electron

excitation. The electron-beam methods are always done in vacuum, of course, whereas XRF and TXRF are done in air. XRF in the WDX mode dominates in terms of the number of systems in use in the world (about 10,000).

In principle all the X-ray emission methods can give chemical state information from small shifts and line shape changes (cf., XPS and AES in Chapter 5). Though done for molecular studies to derive electronic structure information, this type of work is rarely done for materials analysis. The reasons are: the instrumental resolution of commercial systems is not adequate; and the emission lines routinely used for elemental analysis are often not those most useful for chemical shift meas-urements. The latter generally involve shallower levels (narrower natural line widths), meaning longer wavelength (softer) X-ray emission.

6.1 XRF

X-Ray Fluorescence

TING C. HUANG

Contents

Introduction

X-Ray Fluorescence (XRF) is a nondestructive method used for elemental analysis of materials. An X-ray source is used to irradiate the specimen and to cause the elements in the specimen to emit (or fluoresce) their characteristic X rays. A detector system is used to measure the positions of the fluorescent X-ray peaks for qualitative identification of the elements present, and to measure the intensities of the peaks for quantitative determination of the composition. All elements but low-Z elements—H, He, and Li—can be routinely analyzed by XRF.

Since the 1950s XRF has been used extensively for the analysis of solids, powders, and liquids. The technique was extended to analyze thin-film materials in the 1970s. XRF can be used routinely for the simultaneous determination of elemental composition and thickness of thin films. The technique is nondestructive, rapid, precise, and potentially very accurate. The results are in good agreement with other elemental analysis techniques including wet chemical, electron-beam excitation techniques, etc.

Basic Principles

The fundamental principles of XRF can be found in the literature.[1–3] Briefly, X rays are electromagnetic radiation of very high energy (or short wavelength). The unit of measurement for X rays is the angstrom (Å), which is equal to 10^{-8} cm. When an X-ray photon strikes an atom and knocks out an inner shell electron, if the incident photon has energy greater than the binding energy of the inner shell electron, a readjustment occurs in the atom by filling the inner shell vacancy with one of the outer electrons and simultaneously emitting an X-ray photon. The emitted photon (or fluorescent radiation) has the characteristic energy of the difference between the binding energies of the inner and the outer shells. The penetration depth of a high-energy photon into a material is normally in the μm range. (Another method commonly used to produce X rays is electron-beam excitation; the penetration depth of an electron beam is about an order of magnitude smaller than that of X rays. See the articles on EDS and EPMA.)

Measurements of the characteristic X-ray line spectra of a number of elements were first reported by H. G. J. Moseley in 1913. He found that the square root of the frequency of the various X-ray lines exhibited a linear relationship with the atomic number of the element emitting the lines. This fundamental "Moseley law" shows that each element has a characteristic X-ray spectrum and that the wavelengths vary in a regular fashion form one element to another. The wavelengths decrease as the atomic numbers of the elements increase. In addition to the spectra of pure elements, Moseley obtained the spectrum of brass, which showed strong Cu and weak Zn X-ray lines; this was the first XRF analysis. The use of XRF for routine spectrochemical analysis of materials was not carried out, however, until the introduction of modern X-ray equipment in the late 1940s.

Instrumentation

The instrumentation required to carry out XRF measurements normally comprises three major portions: the primary X-ray source, the crystal spectrometer, and the detection system. A schematic X-ray experiment is shown in Figure 1. Fluorescent X rays emitted from the specimen are caused by high-energy (or short-wavelength) incident X rays generated by the X-ray tube. The fluorescent X rays from the specimen travel in a certain direction, pass through the primary collimator. The analyzing crystal, oriented to reflect from a set of crystal planes of known d-spacing, reflects one X-ray wavelength (λ) at a given angle (θ) in accordance with Bragg's law: $n\lambda = 2d\sin\theta$, where n is a small positive integer giving the order of reflection. By rotating the analyzing crystal at one-half the angular speed of the detector, the various wavelengths from the fluorescent X rays are reflected one by one as the analyzing crystal makes the proper angle θ for each wavelength. The intensity of at each wavelength is then recorded by the detector. This procedure is known also as the

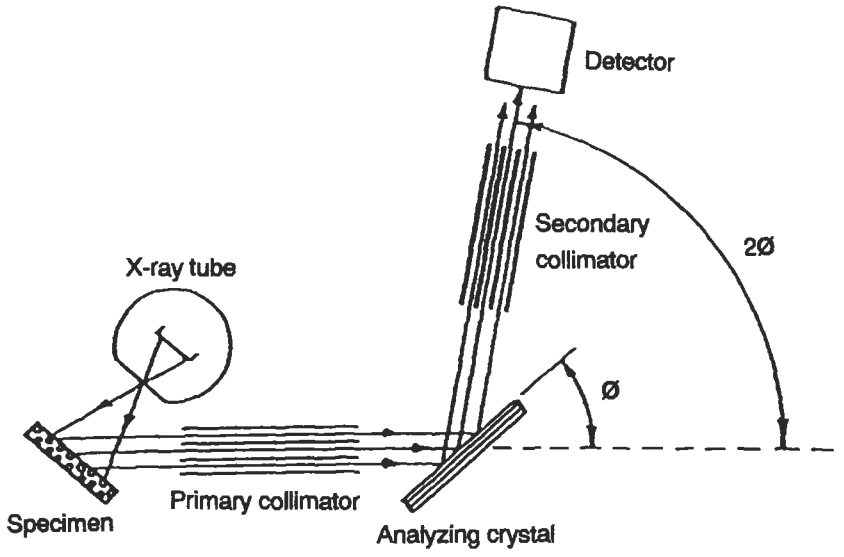

Figure 1 **Schematic of XRF experiment.**

wavelength-dispersive method. (The wavelength-dispersive method is used extensively in EPMA, see the EPMA article in this volume.)

X-RaySources

A sealed X-ray tube having a W, Cu, Rh, Mo, Ag, or Cr target is commonly used as the primary X-ray source to directly excite the specimen. A secondary target material located outside the X-ray tube is used sometimes to excite fluorescence. This has the advantages of selecting the most efficient energy close to the absorption edge of the element to be analyzed and of reducing (or not exciting) interfering elements. (The intensity is much reduced, however.) X-ray sources, including synchrotron radiation and radioactive isotopes like ^{55}Fe (which emits Mn KX rays) and AM-241 (Np LX rays) are used in place of an X-ray tube in some applications.

Analyzing Crystals

Crystals commonly used in XRF are: LiF (200) and (220), which have 2d-spacings of 4.028 and 2.848 Å, respectively; pyrolytic graphite (002), spacing 6.715 Å; PET(002), spacing 8.742 Å; TAP(001), spacing 25.7 Å; and synthetic multilayers of W/Si, W/C, V/C, Ni/C, and Mo/B_4C, spacing 55–160 Å. The lowest-Z element that can be detected and reflected efficiently depends on the d-spacing of the analyzing crystal selected. The crystals are usually mosaic, and each reflection is spread over a small angular range. It is thus important that the crystal used be of good quality to obtain intensive and sharp XRF peaks. The angular spread of the

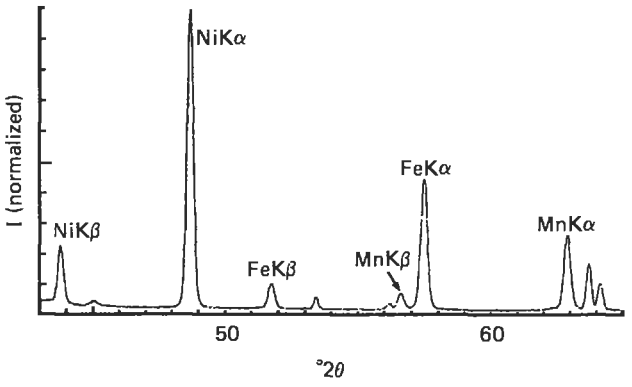

Figure 2 **XRF spectrum of MnFe/NiFe thin film.**

peaks, or the dispersion, $d\theta/d\lambda = n/(2d\cos\theta)$, increases with decreasing d. The dispersion thus can be increased by selecting a crystal with a smaller d.

X-Ray Detection Systems

The detectors generally used are scintillation counters having thin Be windows and NaI–Tl crystals for short wavelengths (above 3 Å or 4 keV), and gas-flow proportional counters having very low absorbing windows and Ar/CH_4 gas for long wavelengths (below 2 Å or 6 keV). A single-channel pulse amplitude analyzer is used to accept fluorescent X rays within a selected wavelength range to improve peak-to-background ratios and to eliminate unwanted high-order reflections.

The counting times required for measurement range between a few seconds and several minutes per element, depending on specimen characteristics and the desired precision.

A typical XRF spectrum of a FeMn/NiFe thin film is plotted in Figure 2. The $K\alpha$ and $K\beta$ XRF fluorescent peaks from the film are identified, and the remaining peaks are those from the spectrum of the X-ray tube. The experimental conditions included a Mo target X-ray tube operated at 45 kV, a LiF (200) analyzing crystal, and a scintillation counter with a single-channel pulse amplitude analyzer. The energy resolution of the Mn Kα peak at 5.89 keV was 24 eV, compared to 145 eV for a Si (Li) solid-state energy-dispersive system (see EDS article). The high spectral resolution of the wavelength-dispersive method made possible the measurements of Ni, Fe, and Mn free of interference from adjacent peaks.

Analytical Capabilities

Elemental Depth Profiling

The X-ray penetration depth in a material depends on the angle of incidence. It increases from a few tens of Å near the total reflection region to several μm at large

incidence angles (a few tens of degrees). The XRF beam, which originates from variable depths, can be used for elemental depth analysis. For example, the grazing incidence XRF method has been used for studies of concentration profiles of a dissolved polymer near the air/liquid interface,[4] Langmuir-Blodgett multilayers,[5] and multiple-layer films on substrates.[6] This type of analysis requires a parallel-incidence beam geometry, which currently is not possible with a conventional spectrometer.

Chemical State Analysis

The XRF wavelengths and relative intensities of a given element are constant to first approximation. Small changes may occur when the distribution of the outer (or valence) electron changes. A major area of research in XRF involves the use of "soft" X-ray emission (or long-wavelength XRF) spectra for chemical state analysis. Soft X-ray peaks often exhibit fine structure, which is a direct indication of the electronic structure (or chemical bonding) around the emitting atom. Thus the shift in peak position, change in intensity distribution, or appearance of additional peaks can be correlated with a variety of chemical factors, including the oxidation state, coordination number, nature of covalently bound ligands, etc. The equipment required for soft X-ray analysis is almost identical to that required for conventional XRF, with one major exception. Since it is a study of transitions involving the outer orbits and therefore long wavelengths, soft X-ray analysis employs a long-wavelength X-ray source such as Al (8.34 Å for Al $K\alpha$) or Cu (13.36 Å for Cu $L\alpha$). Special analyzing crystals or gratings for measuring wavelengths in the range 10–100 Å also are needed.[7]

Quantitative Analysis

In addition to qualitative identification of the elements present, XRF can be used to determine quantitative elemental compositions and layer thicknesses of thin films. In quantitative analysis the observed intensities must be corrected for various factors, including the spectral intensity distribution of the incident X rays, fluorescent yields, matrix enhancements and absorptions, etc. Two general methods used for making these corrections are the empirical parameters method and the fundamental parameters methods.

The empirical parameters method uses simple mathematical approximation equations, whose coefficients (empirical parameters) are predetermined from the experimental intensities and known compositions and thicknesses of thin-film standards. A large number of standards are needed for the predetermination of the empirical parameters before actual analysis of an unknown is possible. Because of the difficulty in obtaining properly calibrated thin-film standards with either the same composition or thickness as the unknown, the use of the empirical parameters method for the routine XRF analysis of thin films is very limited.

The fundamental parameters method uses XRF equations derived directly from first principles. Primary and secondary excitations are taken into account. Primary excitations are caused directly by the incident X rays from the X-ray source, while the secondary excitations are caused by other elements in the same film, whose primary fluorescent X-ray radiation has sufficient energy to excite the characteristic radiation of the analyzed element. Higher order excitations are generally considered insignificant because of their much lower intensities. XRF equations relate intensity, composition, and thickness through physical constants (fundamental parameters) like fluorescent yields, atomic transition probabilities, absorption coefficients, etc. For example, the XRF equations for single-layer films were reported by Laguitton and Parrish,[8] and for multiple-layer films by Mantler.[9] The equations for thin films are very complex, and the values of composition and thickness cannot be determined directly from the observed intensities. They are obtained by computer iteration using either linear or hyperbolic approximation algorithm. The fundamental parameters technique is suitable for the analysis of thin films because it requires a minimum number of pure or mixed element and bulk or thin-film standards.

Applications

The principle application of XRF thin-film analysis is in the simultaneous determination of composition and thickness. The technique has been used for the routine analysis of single-layer films[8] since 1977 and multiple-layer films[10] since 1986. Two main sources of publications in the fields are the annual volumes of *Advances in X-Ray Analysis* by Plenum Press, New York, and the *Journal of X-Ray Spectrometry* by Heyden and Sons, London. Typical examples on the analysis of single-layer films and multiple-layer films are used to illustrate the capabilities of the technique.

Single-Layer Films

Evaporated FeNi films with a large range of compositions were selected because of the strong absorption of Ni and enhancement of Fe KX rays in the films. XRF compositions of 7 FeNi films deposited on quartz substrates are listed in Table 1 and are compared to those obtained by the Atomic Absorption Spectroscopy (AAS) and the Electron Probe Microanalysis (EPMA). Since the strong X-ray absorption and enhancement effects are severe for both XRF and EPMA but not present in AAS, a comparison between the XRF results and the two non-XRF techniques provide a useful evaluation of XRF.[11, 12] As shown in Table 1, there is good agreement between results of XRF and AAS or EPMA, and the average deviation is 0.9% between XRF and AAS and is 1.1% between XRF and EPMA. It is worth noting that the compositions of more than half of the 7 FeNi films obtained by XRF, AAS, and EPMA are significantly different from the intended compositions (see values inside the parentheses listed in column 1 of Table 1). The discrepancy shows the

Film	XRF	AAS	EPMA
Fe (5)–Ni (95)	4.2	5.0	2.5
Fe (10)–Ni (90)	9.2	9.0	6.2
Fe (20)–Ni (80)	19.4	19.2	19.4
Fe (34)–Ni (66)	47.3	48.4	44.5
Fe (50)–Ni (50)	59.1	61.7	59.1
Fe (66)–Ni (34)	78.9	79.8	78.4
Fe (80)–Ni (20)	89.2	89.6	89.2

Table 1 Fe concentrations (% wt.) for FeNi films.

risk of using intended composition and the important of determining composition experimentally by XRF or other reliable techniques.

The volume density ρ and thickness t of a film appear together as a single parameter ρt in the XRF equations, the value of ρt, the areal density (not the thickness) is determined directly by iteration. From the areal density, the film thickness can be calculated when the volume density is known experimentally or theoretically. Using the volume densities calculated from the film composition and the published volume densities of pure elements, the thicknesses of 12 $Fe_{20}Ni_{80}$ films were calculated from the XRF areal densities and are compared to those obtained by a nonXRF technique (i.e., AAS or a deposition monitor). As shown in Table 2, good agreement between XRF and non-XRF thicknesses are obtained with average and maximum deviations of 2.95% and 6.7%, respectively (see the last column of Table 2). The volume density can also be calculated from the XRF areal density when the thickness of a film is known. For example, the volume densities of 8 $Fe_{19}Ni_{81}$ permalloy films with known thicknesses of 50–10,000 Å were calculated from the XRF areal densities. The calculation shows that the volume density of the permalloy is not constant and changes systematically with the film's thickness. It is equal to the bulk value of 8.75 g/cm^3 for films of 1000 Å or greater thickness, decreases to 94% of the bulk value for the 500-Å film, and to 81% for the 50-Å film.[12]

Multiple-layer Films

XRF analysis of multiple-layer films is very complex because of the presence of XRF absorption and enhancement effects, not only between elements in the same layer but also between all layers in the film. Equations for the calculation of XRF intensities for multiple-layer films are available from the literature.[9, 13] Proper correc-

Film	XRF	Non-XRF[a]	Δ/XRF (%)[b]
1	825	848	2.8
2	858	848	1.2
3	1117	1142	2.2
4	3180	2967	6.7
5	3215	3011	6.3
6	3558	3473	2.4
7	3579	3524	1.5
8	4090	4070	0.5
9	5533	5452	1.5
10	5550	5237	5.6
11	5601	5655	1.0
12	6283	6053	3.7

a. Either AAS or monitor.
b. Δ = |XRF – non-XRF|.

Table 2 **Thicknesses (Å) for $Fe_{20}Ni_{80}$ films.**

tions for intralayer and interlayer effects are essential for a successful XRF analysis of multiple-layer films. The accuracy of XRF compositions and thicknesses for multiple-layer films was found to be equal to those for single-layer films.

For example, XRF was used successfully to analyze two triple-layer films of Cr, Cu, and FeNi deposited on Si substrates.[10, 12, 14] The two films, T1 and T2, have identical individual Cr, Cu and FeNi layers but different order. In T1, the FeNi layer is on top, the Cu layer in the middle, and the Cr layer at the bottom; in T2, the positions of the Cr and FeNi layers are reversed, with Cr on top and FeNi at the bottom; meanwhile the Cu layer remains in the middle. Because of this reversal of layer order, interlayer absorption and enhancement effects are grossly different between these two films. This led to large differences in the observed intensities between these two films. The differences between T1 and T2 were –17%, +2%, +20%, and +15%, respectively, for the Cr, Cu, Fe, and Ni Kα observed intensities.[12] Using the same set of observed XRF intensities, the results obtained by two different analysis programs: LAMA-III from the US[12] and DF270 from Japan[14] are essentially the same within a relative deviation of 0.2% in composition and 1% in

Parameter	Triple layer		Single layer		
	T1 (FeNi/Cu/Cr)	T2 (Cr/Cu/FeNi)	S1 (Cr)	S2 (FeNi)	S3 (Cu)
Fe (% wt.)	10.25	10.25	—	10.50	—
Ni (% wt.)	89.75	89.75	—	89.50	—
t_{Cr} (Å)	1652	1698	1674	—	—
t_{FeNi}(Å)	2121	2048	—	2115	—
t_{Cu}(Å)	2470	2457	—	—	2416

Table 3 **XRF results for films of Cr, FeNi, and Cu.**

thickness. The results obtained by the LAMA-III program are listed in Table 3. In spite of the large differences in the observed intensities of Cr, Fe and Ni, the compositions and thickness of all three layers determined by XRF are essentially the same for T1 and T2. For comparison, an XRF analysis was also done on three single-layer Cr, FeNi, and Cu films (S1, S2, and S3) prepared under identical deposition conditions to the two triple-layer films. As shown in Table 3, good agreement was obtained between the single- and triple-layer films. This indicates that the severe interlayer enhancement and absorption effects observed in T1 and T2 were corrected properly. It is also worth noting that the deviations between the results of the triple- and single-layer films are within the accuracy reported for the single-layer films.

In multiple-layer thin films, it is possible that some of the elements may be present simultaneously in two or more layers. XRF analysis of this type of film can be complicated and cannot be made solely from their observed intensities. Additional information, such as the compositions or thickness of some of the layers is needed. The amount of additional non-XRF information required depends on the complexity of the film. For example, in the analysis of a FeMn/NiFe double-layer film, the additional information needed can be the composition or thickness of either the FeMn or NiFe layer. Using the composition or thickness of one of the film predetermined from a single-layer film deposited under identical conditions, XRF analysis of the FeMn/NiFe film was successful.[12]

Related Techniques

XRF is closely related to the EPMA, energy-dispersive X-Ray Spectroscopy (EDS), and total reflection X-Ray Fluorescence (TRXF), which are described elsewhere in this encyclopedia. Brief comparisons between XRF and each of these three techniques are given below.

EPMA

Both XRF and EPMA are used for elemental analysis of thin films. XRF uses a non-focusing X-ray source, while EPMA uses a focusing electron beam to generate fluorescent X rays. XRF gives information over a large area, up to cm in diameter, while EPMA samples small spots, μm in size. An important use of EPMA is in point-to-point analysis of elemental distribution. Microanalysis on a sub-μm scale can be done with electron microscopes. The penetration depth for an X-ray beam is normally in the 10-μm range, while it is around 1 μm for an electron beam. There is, therefore, also a difference in the depth of material analyzed by XRF and EPMA.

EDS

EDS is another widely used elemental analysis technique and employs a solid state detector with a multichannel analyzer to detect and resolve fluorescent X rays according to their energies. EDS uses either X rays or an electron beam as a source to excite fluorescence. Unlike XRF, which uses the wavelength-dispersive method to record X-ray intensities one by one, EDS collects all the fluorescent X rays from a specimen simultaneously. A limitation of EDS is its energy resolution, which is an order of magnitude poorer than that of the wavelength-dispersive method. For example, the Kα peaks of transition elements overlap the Kβ peaks of the next lighter element, which cause analytical difficulties. The poorer resolution also causes relatively lower peak-to-background ratios in EDS data.

TXRF

XRF at large incident angles, as described in this article, is normally used for elemental analysis of major concentrations of 0.1% or higher. Total Reflection X-Ray Fluorescence (TXRF) with grazing-incidence angles of a few tenths of a degree is used for trace-element analysis. Detectable limits down to 10^9 atoms/cm^2 are now attainable using a monochromatic X-ray source. Examples of the use of this technique in wafer technology are given in the article on TXRF in this volume.

Conclusions

XRF is one of the most powerful analysis technique for the elemental-composition and layer-thickness determination of thin-film materials. The technique is nondestructive, inexpensive, rapid, precise and potentially very accurate. XRF characterization of thin films is important for the research, development, and manufacture of electronic, magnetic, optical, semiconducting, superconducting, and other types of high-technology materials. Future development is expected in the area of microbeam XRF, scanning XRF microscopy, grazing-incidence XRF analysis of surfaces and buried interfaces, long-wavelength XRF and chemical state analysis, and synchrotron XRF.

Related Articles in the Encyclopedia

EPMA, EDS, and TXRF

References

1 L. S. Birks. *X-Ray Spectrochemical Analysis.* Second Edition, Wiley, New York, 1969. A brief introduction to XRF, it will be useful to those who are interested in knowing enough about the technique to be able to use it for routine analysis. A separate chapter on EPMA also is included.

2 E. P. Bertin. *Principles and Practice X-Ray Spectrometric Analysis.* Plenum, New York, 1970. A practical textbook that also serves as a laboratory handbook, although somewhat dated.

3 R. Jenkins. *An Introduction to X-Ray Spectrometry.* Heyden, London, 1974. A good introduction to XRF instrumentation, qualitative and quantitative analyses, and chemical-bonding studies.

4 J. M. Bloch, M. Sansone, F. Rondelez, D. G. Peiffer, P. Pincus, M. W. Kim, and P. M. Eisenberger. *Phys. Rev. Lett.* **54,** 1039, 1985.

5 M. J. Bedzyk, G. M. Bommarito, and J. S. Schidkraut. *Phys. Rev. Lett.* **62,** 1376, 1989.

6 D. K. G. de Boer. In *Advances in X-Ray Analysis.* (C. S. Barrett et al., Eds.) Plenum, New York, 1991, Vol. 34, p. 35.

7 B. L. Henke, J. B. Newkirk, and G. R. Mallet, Eds. *Advances in X-Ray Analysis.* Plenum, New York, 1970, Vol. 13. The proceedings of the 18th Annual Denver Conference on Applications of X-ray Analysis; the central theme of the Conference was interactions and applications of low-energy X-rays.

8 D. Laguitton and W. Parrish. *Anal. Chem.* **49,** 1152, 1977.

9 M. Mantler. *Anal. Chim. Acta.* **188,** 25, 1986.

10 T. C. Huang and W. Parrish. In *Advances in X-Ray Analysis.* (C. S. Barrett, et al., Eds.) Plenum, New York, 1986, Vol. 29, p. 395.

11 T. C. Huang and W. Parrish. In *Advances in X-Ray Analysis.* (G. J. McCarthy et al., Eds.) Plenum, New York, 1979, Vol. 22, p. 43.

12 T. C. Huang. *Thin Solid Films.* **157,** 283, 1988; and *X-Ray Spect.* **20,** 29, 1991.

13 D. K. G. de Boer. *X-ray Spect.* **19,** 145, 1990.

14 Y. Kataoka and T. Arai. In *Advances in X-Ray Analysis.* (C. S. Barrett et al., Eds.) Plenum, New York, 1990, Vol. 33, p. 220.

6.2 TXRF

Total Reflection X-Ray Fluorescence Analysis

PETER EICHINGER

Contents

Introduction

X-Ray Fluorescence analysis (XRF) is a well-established instrumental technique for quantitative analysis of the composition of solids. It is basically a bulk evaluation method, its analytical depth being determined by the penetration depth of the impinging X-ray radiation and the escape depth of the characteristic fluorescence quanta. Sensitivities in the ppma range are obtained, and the analysis of the emitted radiation is mostly performed using crystal spectrometers, i.e., by wavelength-dispersive spectroscopy. XRF is applied to a wide range of materials, among them metals, alloys, minerals, and ceramics.

In the total reflection mode, with the X rays impinging at a grazing angle onto a specular solid surface, interference between the incident and the reflected X-ray waves limits the excitation depth to a few monatomic layers in which the radiation intensity is locally concentrated. Accordingly this surface sheet, which has a depth of a few nm, is strongly excited, giving rise to an intensive emission of fluorescence quanta. The bulk of the solid is virtually decoupled by the total reflection, leading to a suppression of matrix background fluorescence radiation. The high sensitivity

of TXRF for surface impurities is a result of both effects: compression of the X-ray intensity in the surface sheet, and suppression of the bulk fluorescence background.

TXRF is essentially a surface-analytical technique, used to detect trace amounts of impurities on specular surfaces. Until a few years ago, its application was limited to the analysis of liquids that have been pipetted in microliter volumes on flat quartz substrates and allowed to dry. Subsequent TXRF of the droplet residue presents an attractive, multielement analysis with sensitivities down to the pg level. The main applications of this branch of TXRF are in environmental research. In recent years the application of TXRF has been expanded to semiconductor technology, with its stringent demands for surface purity, especially with respect to heavy-metal contamination.[1] In this application, the semiconductor substrate is directly subjected to TXRF. Detection limits on the order of 10^{10} metal atoms per cm^2, corresponding to 10 ppma of a monatomic surface layer, are obtained on silicon wafers using a monochromatic X-ray source. The following sections focus on the instrumentation and application of TXRF to semiconductor substrates that are usually electrochemically polished and thus provide ideal conditions for TXRF; the wafer's relatively large diameter allows for automatic adjustment of the critical angle. Dedicated wafer surface analyzers are on the verge of becoming routine monitoring tools in the semiconductor industry.

Principles of Direct TXRF

The primary X-ray beam is directed onto the solid surface in grazing incidence. The angle of incidence is kept below the critical angle at which total reflection occurs. The critical angle is given by

$$\phi_C = 3.72\times10^{-11}\frac{\sqrt{n_e}}{E} \qquad (1)$$

where ϕ_C is the critical angle (mrad), n_e is the electron density (cm^{-3}), and E is the quantum energy (keV). The critical angle ϕ_C is inversely proportional to the energy of the X-ray quanta, and increases with the square root of the electron density of the solid. For molybdenum K_α-radiation and a silicon surface, ϕ_C is 1.8 mrad.

The angular dependence of the fluorescence yield in the neighborhood of the critical angle should be considered in detail to establish the chemical nature of surface impurities, as well as for quantitation in terms of their concentrations (Figure 1).

Agglomerated impurities, such as particles or droplet residues, do not participate in the interference phenomenon leading to total reflection; their fluorescence intensity is independent of the angle of incidence below the critical angle, and drops by a factor of 2 if the critical angle is surpassed due to the disappearance of the reflected component in the exciting beam (*nonreflecting* impurities and *residues*).

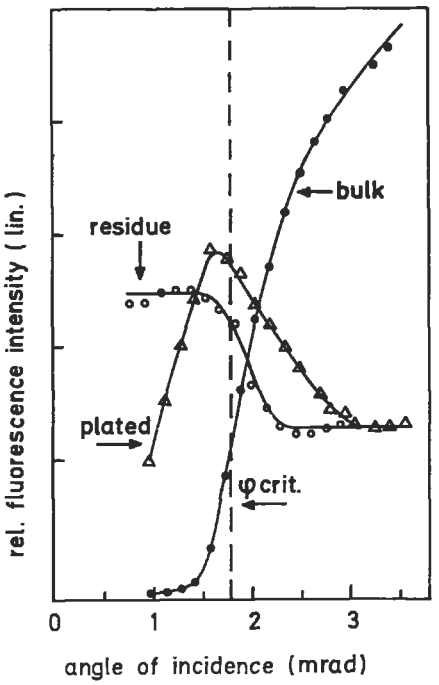

Figure 1 **Experimental curves for the angular dependence of the fluorescence intensity from plated or sputtered submonatomic Ni layers (open triangles), layers produced by the evaporation of a Ni salt solution (open circles), and the silicon substrate (filled circles).**

On the other hand, impurities that are homogeneously distributed through a submonatomic layer within the surface, such as electrochemically plated, sputtered, or evaporated atoms, are part of the reflecting surface and their fluorescent yield shows a pronounced dependence on the incidence angle. These *reflecting* or *plated* impurities exhibit basically the same angular dependence below the critical angle as the matrix fluorescence from the bulk silicon, but they peak at the critical angle.

The plated-type impurities are most commonly encountered with semiconductor substrates; they originate, for example, from wet chemical processing steps. It is apparent from Figure 1 that a precise control of the angle of incidence is an essential feature of TXRF instrumentation.

X-Ray Sources

Sealed conventional fine structure tubes with Mo, W, Cu, or Cr anodes are used as primary X-ray sources, as well as rotating anode tubes, or synchrotron radiation. The maximum energy of the X-ray quanta determines the range of elements acces-

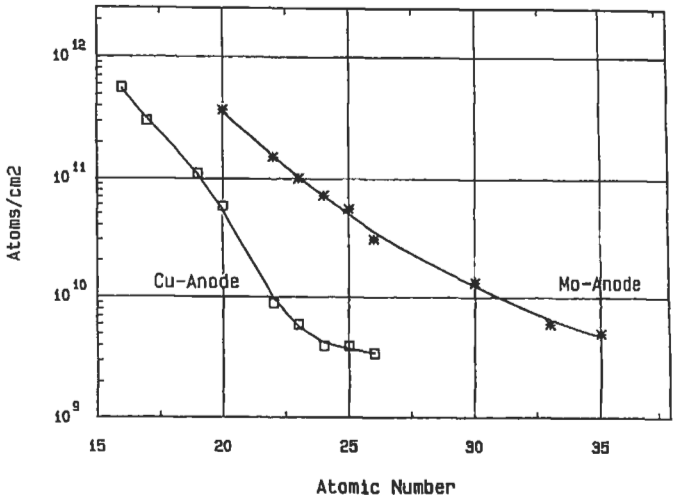

Figure 2 **Detection limits obtained with Cu and Mo anodes in conjunction with a monochromator.[2]**

sible for analysis and the detection limits of the respective elements, as shown in Figure 2 for monochromatized radiation from a Cu and Mo anode. In this example, Fe ($Z = 26$) can be detected at a level below 10^{10} atoms/cm^2 using the Cu anode, but Cu is not detectable.

In modern TXRF instrumentation, the primary radiation from the X-ray tube is filtered or monochromatized to reduce the background originating primarily from bremsstrahlung quanta with higher energy than the main characteristic line for the anode material. The higher energy radiation does not fulfill the critical angle condition for total reflection and penetrates into the substrate, thus adding scattered radiation. Energy filtering is achieved using multilayer interference or crystal diffraction.

VPD-TXRF

The term *direct TXRF* refers to surface impurity analysis with no surface preparation, as described above, achieving detection limits of 10^{10}–10^{11} cm^{-2} for heavy-metal atoms on the silicon surface. The increasing complexity of integrated circuits fabricated from silicon wafers will demand even greater surface purity in the future, with accordingly better detection limits in analytical techniques. Detection limits of less than 10^9 cm^{-2} can be achieved, for example, for Fe, using a preconcentration technique known as Vapor Phase Decomposition (VPD).

The VPD method originally was developed to determine metal trace impurities on thermally oxidized or bare silicon surfaces in combination with atomic absorp-

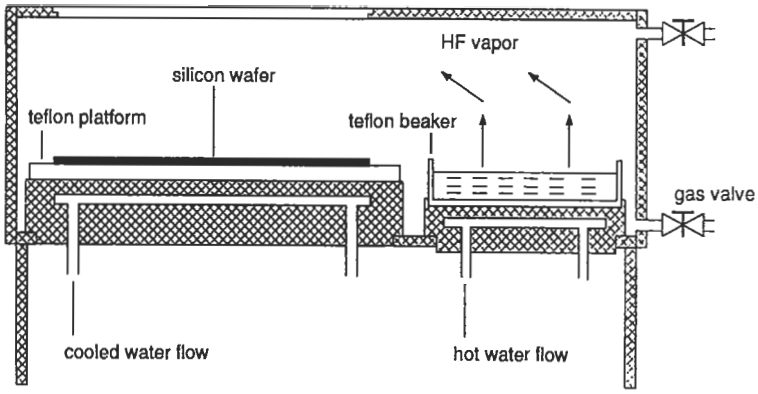

Figure 3 **Schematic arrangement for vapor phase decomposition (VPD) applied to silicon wafers.**

tion spectroscopy (VPD-AAS). The silicon wafer is exposed to the vapor of hydrofluoric acid, which dissolves the SiO_2 surface layer (native or thermal oxide) according to the reaction:

$$SiO_2 + 6HF \rightarrow H_2SiF_6 + 2H_2O \quad (2)$$

The impurities on the surface are contained in the resulting water droplet or moisture film, and are collected *in situ* for further investigation by scanning the surface with an auxiliary water droplet (e.g., 50 µl). The VPD residue is allowed to dry in the center of the wafer and subjected to TXRF analysis. A schematic of a VPD reactor is shown in Figure 3.

With VPD preconcentration, the angular dependence of the impurity fluorescence yield follows the curve for residue impurities, as shown in Figure 1, in contrast to the plated-impurity case using direct TXRF.

The sensitivity enhancement achieved by VPD is determined by the ratio of the substrate area to the area of the detector aperture (analyzed area), provided there is full collection of the impurities. This has been demonstrated for Fe and Zn. For Cu and Au, however, only a small percentage can be collected using this technique,[3] due to electrochemical plating. An example comparing direct TXRF with VPD-TXRF on the same substrate is shown in Figure 4.

Semiconductor Applications

In silicon integrated circuit technology, TXRF analysis is applied as a diagnostic tool for heavy-metal contamination in a variety of process steps, including incoming wafer control, preoxidation cleaning, and dry processing equipment evaluation. As an example, Figure 5 shows the effect of applying a standard cleaning to silicon

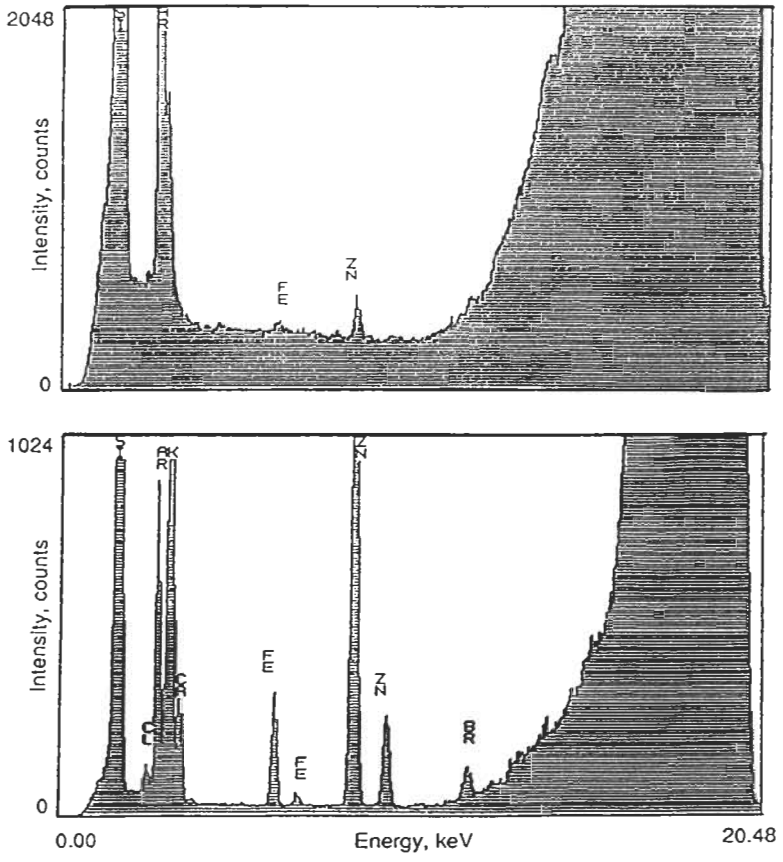

Figure 4 **Direct TXRF (upper spectrum, recording time 3000 s) and VPD-TXRF (lower spectrum, recording time 300 s) on a silicon wafer surface. The sensitivity enhancement for Zn and Fe is two orders of magnitude. The measurements were made with a nonmonochromatized instrument.**

wafers received from a commercial vendor: The contamination is similar for wafers 1, 2, and 3, with K, Ca, Fe, and Zn as the predominant metal impurities in concentrations of 10^{11}–10^{12} atoms/cm^2. Cleaning on wafers 4, 5, and 6 removes all metals to a level of less than 10^{10} cm^{-2}, except for Fe which is still detectable. The deposition of Br is due to the cleaning solution and is not considered harmful. The analysis has been performed using VPD-TXRF.

With gallium arsenide, additional elements, such as Si, S, and Cl, are of interest because of their doping character. Impurity levels on the order of 10^{12} cm^{-2} are encountered with commercial substrates, which can be readily assessed using direct TXRF.[4] VPD-TXRF is not possible in this case because of the lack of a native oxide layer on gallium arsenide.

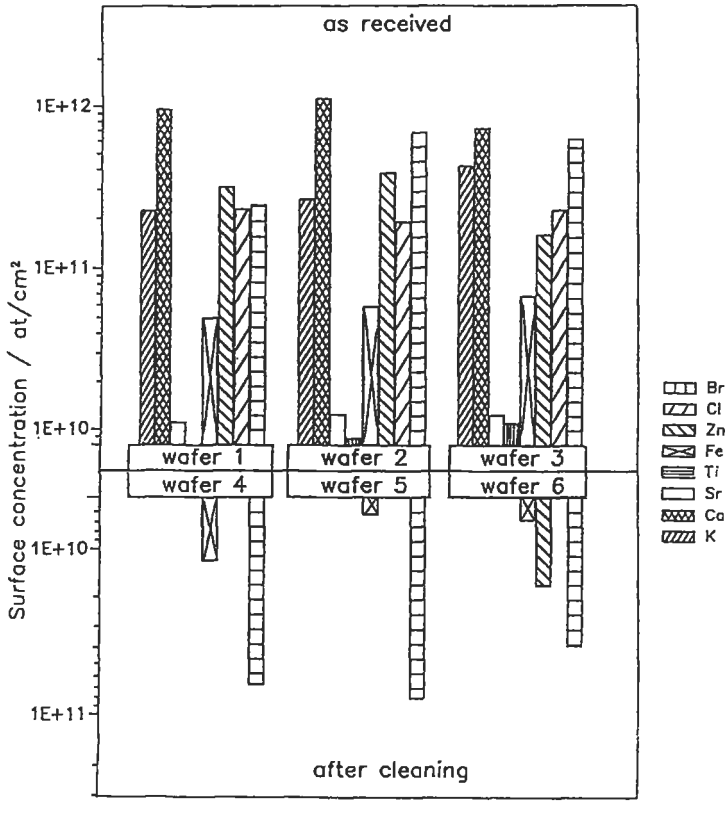

Figure 5 **Effect of cleaning on the surface purity of silicon wafers, as measured by VPD-TXRF.**

Comparative Techniques

Atomic absorption spectroscopy of VPD solutions (VPD-AAS) and instrumental neutron activation analysis (INAA) offer similar detection limits for metallic impurities with silicon substrates. The main advantage of TXRF, compared to VPD-AAS, is its multielement capability; AAS is a sequential technique that requires a specific lamp to detect each element. Furthermore, the problem of blank values is of little importance with TXRF because no handling of the analytical solution is involved. On the other hand, adequately sensitive detection of sodium is possible only by using VPD-AAS. INAA is basically a bulk analysis technique, while TXRF is sensitive only to the surface. In addition, TXRF is fast, with an typical analysis time of 1000 s; turn-around times for INAA are on the order of weeks. Gallium arsenide surfaces can be analyzed neither by AAS nor by INAA.

Conclusions

Triggered by the purity demands of silicon integrated circuit technology, TXRF has seen a rapid development in its application to solid surfaces during the last seven years, which is reflected in the availability of a variety of commercial instruments and services today. The investigation of surface cleanliness, however, does not exhaust the inherent capabilities of TXRF: From the detailed angular dependence of the fluorescence yields around the critical angle for total reflection, information may be obtained about thin films, interfaces, or multilayer structures in the future. An overview of these trends can be found in *Proceedings of the International Workshop on Total Reflection X-Ray Fluorescence.*[5] It is also possible, in principle, to obtain chemical state information, along with elemental analysis. This requires the use of high-energy resolution techniques to detect small shifts in line positions in the emitted fluorescence. In the soft X-ray region, instrumentation of this type is not commercially available.

Related Articles in the Encyclopedia

XRF and NAA

References

1 P. Eichinger, H. J. Rath, and H. Schwenke. In: *Semiconductor Fabrication: Technology and Metrology. ASTM STP 990.* (D. C. Gupta, ed.) American Society for Testing and Materials, 305, 1989.

2 U. Weisbrod, R. Gutschke, J. Knoth, and H. Schwenke. *Fresenius J. Anal. Chem.* 1991, in press.

3 C. Neumann and P. Eichinger. *Spectrochimica Acta B At. Spect.* **46,** Vol. 10, 1369, 1991.

4 R. S. Hockett, J. Metz, and J. P. Tower. *Proceedings of the Fifth Conference on Semi-Insulating III-V Materials.* Toronto, 1990.

5 *Proceedings of the International Workshop on Total Reflection X-Ray Fluorescence.* Vienna, 1990 (same as Reference 3).

6.3 PIXE

Particle-Induced X-Ray Emission

RONALD G. MUSKET

Contents

Introduction

Particle-Induced X-Ray emission (PIXE) is a quantitative, nondestructive analysis technique that relies on the spectrometry of characteristic X rays emitted when high-energy particles (~0.3–10 MeV) ionize atoms of a specimen. PIXE provides simultaneous analysis of many elements with sensitivity and detection limits that compare very favorably with other techniques. Since the first quantitative measurements of thin metal films in the late 1960s, PIXE has been applied successfully in a variety of fields, including corrosion and oxidation, semiconductors, metallurgy, thin films, geoscience, air pollution and atmospheric science, biology, medicine, art, archaeology, water analysis, and forensic science. During this 25-year period, PIXE has matured and developed into a routine analytical tool for many applications. A recent survey of over a hundred PIXE systems throughout the world revealed that the main areas of application are currently biomedicine (a major application for 40% of the systems), materials (30%) and aerosols (20%).[1] A detailed discussion of PIXE is presented in the recent book by Johansson and Campbell,[2] which was a major reference for this article.

Generally the particles used for PIXE are protons and helium ions. PIXE is one of three techniques that rely on the spectrometry of X rays emitted during irradiation of a specimen. The other techniques use irradiation by electrons (electron microprobe analysis, EMPA, and energy-dispersive X rays, EDS) and photons (X-Ray Fluorescence, XRF). In principle, each of these techniques can be used to analyze simultaneously for a large range of elements—from lithium to uranium. For simultaneous, multi-elemental determinations using a standard energy-dispersive, X-ray spectrometer, the range of elements is reduced to those with atomic number $Z > 11$. Analysis for elements with $Z > 5$ can be performed with windowless or high transmission-windowed detectors. Wavelength-dispersive detection systems can be used for high-resolution X-ray spectrometry of, at most, a few elements at a time; however, the improved resolution yields information on the chemical bonding of the element monitored. In this article only the results from the widely used lithium-drifted, silicon—Si(Li)—energy-dispersive spectrometers will be discussed. (See also the article on EDS.)

Compared to EDS, which uses 10–100 keV electrons, PIXE provides orders-of-magnitude improvement in the detection limits for trace elements. This is a consequence of the much reduced background associated with the deceleration of ions (called *bremsstrahlung*) compared to that generated by the stopping of the electrons, and of the similarity of the cross sections for ionizing atoms by ions and electrons. Detailed comparison of PIXE with XRF showed that PIXE should be preferred for the analysis of thin samples, surface layers, and samples with limited amounts of materials.[3] XRF is better for bulk analysis and thick specimens because the somewhat shallow penetration of the ions (e.g., tens of μm for protons) limits the analytical volume in PIXE.

Basic Principles

The X-ray spectrum observed in PIXE depends on the occurrence of several processes in the specimen. An ion is slowed by small inelastic scatterings with the electrons of the material, and it's energy is continuously reduced as a function of depth (see also the articles on RBS and ERS, where this part of the process is identical). The probability of ionizing an atomic shell of an element at a given depth of the material is proportional to the product of the cross section for subshell ionization by the ion at the reduced energy, the fluorescence yield, and the concentration of the element at the depth. The probability for X-ray emission from the ionized subshell is given by the fluorescence yield. The escape of X rays from the specimen and their detection by the spectrometer are controlled by the photoelectric absorption processes in the material and the energy-dependent efficiency of the spectrometer.

Interactions of Ions With Materials

After monoenergetic protons and helium ions having energies between about 0.3 and 10 MeV enter a material, they begin slowing down by inelastically scattering

with electrons and elastically scattering with atomic nuclei. The statistical nature of this slowing process leads to a distribution of implanted ions about a mean depth called the projected range R_p, which has a standard deviation ΔR_p. These losses and ranges can be evaluated for various combinations of incident ion and target material using well-developed calculational procedures, such as the Monte Carlo code called TRIM (transport of ions in materials).[4]

When the velocity of the ions is much greater than that of the bound electrons, interactions with the electrons dominate and the ion path can be considered to be a straight line. At any depth associated with the straight-line part of the trajectory, the number of ions is preserved because only about one ion in a million is backscattered; however, their energies decrease slowly and spread increasingly about the average as a result of interactions with the electrons. This energy regime corresponds to that of the dominant X-ray production cross sections; thus modeling the source term for X rays is much simpler for ions than for electrons, which undergo strong deviations from their initial flight path as a result of collisions with the electrons of the target.

X-Ray Production

Although there have been various theoretical schemes for calculating cross sections for inner-shell ionizations by protons and helium ions, many PIXE workers now use the *K*- and *L*-shell cross sections calculated using the ECPSSR method. This method involves a series of modifications to the plane-wave Born approximation, which uses perturbation theory to describe the transition from an initial state consisting of a plane-wave projectile and a bound atomic electron to a final state consisting of a plane-wave particle and an ejected continuum electron. The ECPSSR method includes the deflection and velocity changes of the projectile caused by energy losses, the Coulomb field of the target nucleus, perturbation of the atomic stationary states, and relativistic effects.[5]

A tabulation[6] of the ECPSSR cross sections for proton and helium-ion ionization of *K* and *L* levels in atoms can be used for calculations related to PIXE measurements. Some representative X-ray production cross sections, which are the product of the ionization cross sections and the fluorescence yields, are displayed in Figure 1. Although these *K*-shell cross sections have been found to agree with available experimental values within 10%, which is adequate for standardless PIXE, the accuracy of the *L*-shell cross sections is limited mainly by the uncertainties in the various *L*-shell fluorescence yields. Knowledge of these yields is necessary to convert X-ray ionization cross sections to production cross sections. Of course, these same uncertainties apply to the EMPA, EDS, and XRF techniques. The *M*-shell situation is even more complicated.

The production of characteristic X rays is determined by the cross sections discussed above, but the observed X-ray spectra include both these characteristic peaks and a continuous background radiation. A detailed investigation of the origin of

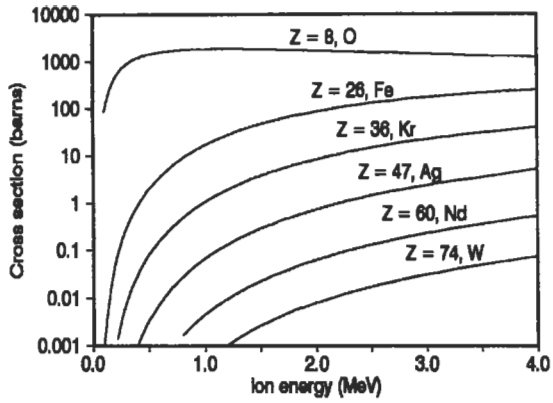

Figure 1 **Calculated *K* X-ray production cross sections for protons using the tabulated ECPSSR ionization cross sections of Cohen and Harrigan,[6] and the fluorescence yields calculated as in Johansson et al.[2] (1 barn = 10^{-24} cm^2).**

this background radiation has shown that the dominant source is the bremsstrahlung radiation emitted by the energetic electrons ejected by the ions.[7] The contributions to the background from electron and proton bremsstrahlung radiation caused by 3-MeV protons are shown in Figure 2. Deviations of the experimental results from the calculated curves for X-ray energies above 10 keV probably represent the effects of Compton scattering of γ rays from excited nuclear states, which were not accounted for in the calculations. In a classical sense, the maximum energy T_m that a 3-MeV proton can transfer to a free electron is 6.5 keV. Thus, in Figure 2 the bremsstrahlung radiation is most intense below T_m and decreases rapidly at higher energies.

From an analytical point of view, this discussion implies that changing the ion energy will not improve the characteristic-to-background (C/B) ratio for X rays having energies below about T_m because both the dominant bremsstrahlung background and the characteristic X rays result from essentially the same ionization processes. However, reducing the ion energy will shift the electron bremsstrahlung radiation to lower energies and have the effect of improving the C/B ratio (i.e., improving the detection limit) for X-ray peaks at energies above T_m. Many PIXE workers prefer 2–3 MeV protons because they provide a reasonable compromise between the characteristic X-ray production rate and the C/B ratio, while limiting the level of background from nuclear reactions. In fact, most modern ion accelerators used for materials analysis can provide protons with maximum energies of 2–4 MeV.

Detection Limits

In PIXE the X-ray spectrum represents the integral of X-ray production along the path length of the decelerating ion, as mediated by X-ray absorption in the mate-

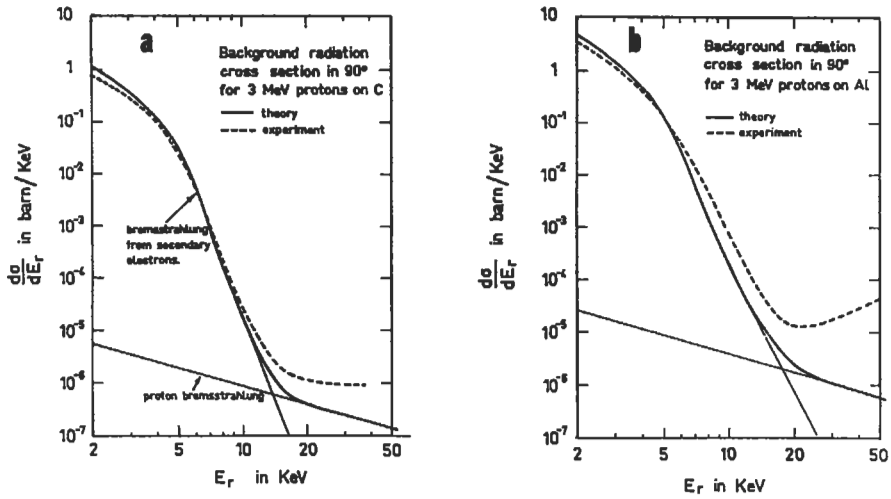

Figure 2 **Experimental and calculated background radiation production cross sections for (a) 360 μg/cm² plastic foil and (b) 200 μg/cm² Al foil.[7]**

rial. Consequently, it is convenient to consider trace analysis for three different cases: thin, free-standing specimens; surface layers (e.g., oxides or coatings) on thick specimens; and thick or bulk specimens.

Specimens are considered thin if an ion loses an insignificant amount of energy during its passage through the foil and if X-ray absorption by the specimen may be neglected. Under these circumstances, the yield of the characteristic X rays can be determined using the ionization cross sections for the energy of the incident ion, and detailed knowledge of the complete composition of the specimen is not needed to make corrections for the particle's energy loss or the absorption of X rays. As shown in Figure 3,[8] the detection limits for various elements in thin specimens depends on the host matrix. About 0.1 weight part per million (wppm) of elements with atomic numbers near 35 and near 80 can be detected in carbon. Thus, less than 10^{-12} g could be detected in or on a 100 μg/cm² carbon foil using a 1-mm² beam of 3-MeV protons.

The detection of impurities or surface layers (e.g., oxides) on thick specimens is a special situation. Although the X-ray production and absorption assumptions used for thin specimens apply, the X-ray spectra are complicated by the background and characteristic X rays generated in the thick specimen. Consequently, the absolute detection limits are not as good as those given above for thin specimens. However, the detection limits compare very favorably with other surface analysis techniques, and the results can be quantified easily. To date there has not been any systematic study of the detection limits for elements on surfaces; however, representative studies have shown that detectable surface concentrations for carbon and

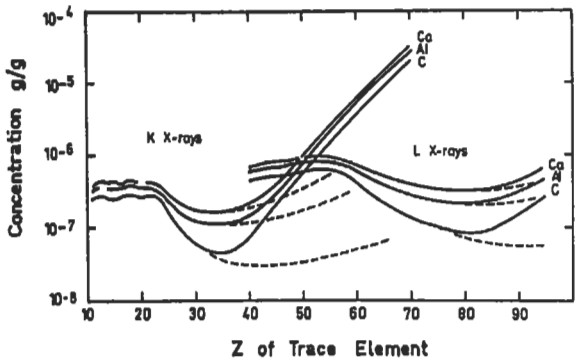

Figure 3 **Calculated detection limits for trace elements in 1 mg/cm^2 specimens of carbon, aluminum, and calcium (100 μC of 3-MeV protons).[8] The dashed curves represent the detection limits if the background radiation is due only to secondary electron bremsstrahlung.**

oxygen are about 100 ng C/cm^2 on iron using 5-MeV He^9 and 30 ng O/cm^2 on beryllium using 2-MeV He.[10]

In thick specimens, the particles ionize atoms along essentially their entire path in the specimen, and calculation of the characteristic X-ray production requires integration of energy-dependent cross sections over all ion energies from the incident energy to 0 and correction for the absorption of the X rays. Detection limits have been estimated for thick targets when the characteristic K X-ray signal occurs at an energy greater than the bremsstrahlung background (Figure 4). For thick targets,[11] limits below 100 ppm are achievable for elements with $Z > 20$ in most matrices and can be below 1 ppm for elements near $Z = 35$ in low-Z matrices; for elements with $Z < 20$, the limits are no better than 100 ppm in most matrices, but can be considerably better in low-Z matrices. For example, a detection limit of 10 ppm for oxygen in beryllium has been demonstrated.[10]

Modes of Analysis

Thin, Free-Standing Specimens

Whenever the appropriate specimens can be prepared, this mode is normally the one preferred for trace-element analysis in geoscience, air pollution and atmospheric science, biology, medicine, water analysis, and forensic science. In this case, the ions pass through the specimen with negligible energy loss and there is minimal absorption of X rays.

Surface Layers on Bulk Specimens

Included in this class of thin surface films are oxides, corrosion, contamination, and deposited layers. Although the presence of the bulk specimen results in increased

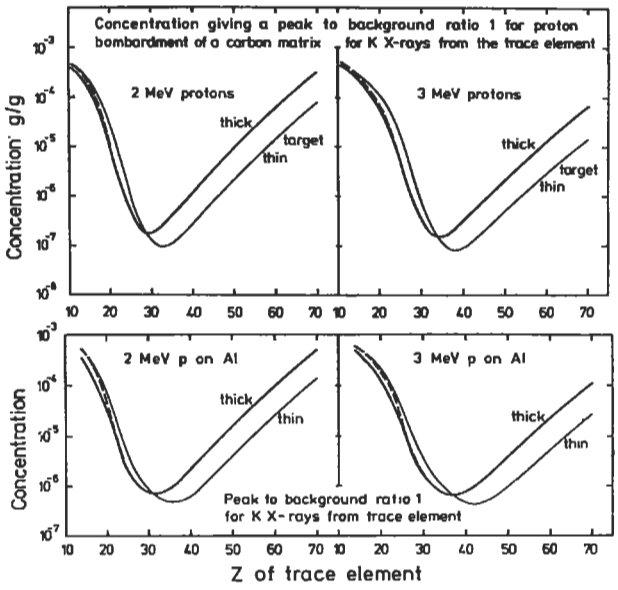

Figure 4 **Calculated minimum concentration of a trace element in thin and thick carbon and aluminum specimens for 2- and 3-MeV protons.[8] The dashed curves show the effects of X-ray absorption on detection limits for thick targets (take-off angle of 45°).**

background radiation compared to that for thin, free standing specimens, the detection limits can be sufficiently low to permit calibration of "true" surface analysis techniques, such as Auger electron spectroscopy (AES). In this sense, PIXE fills the "quantitative gap" that exists in surface and thin-film analysis. As an example, Figure 5[12] shows the helium-induced X-ray spectrum for an anodized tantalum specimen typical of those used to define the sputtering conditions for AES depth profiling experiments. This represents the simplest surface-layer case because the element of interest in the surface layer (i.e., oxygen) is not measurable in the bulk. Thus, the O–*K* X-ray signal can be directly related to the surface concentration of the oxygen.

Bulk Material

Although XRF is generally the X-ray spectrometry method of choice for analysis of major and trace elements in bulk specimens, useful PIXE measurements can be made. A detailed review of the main considerations for thick-target PIXE[11] provides guidance for trace analysis with known and unknown matrices and bulk analysis when the constituents are unknown. Campbell and Cookson[11] also discuss the increased importance of secondary fluorescence and geometrical accuracy for bulk measurements.

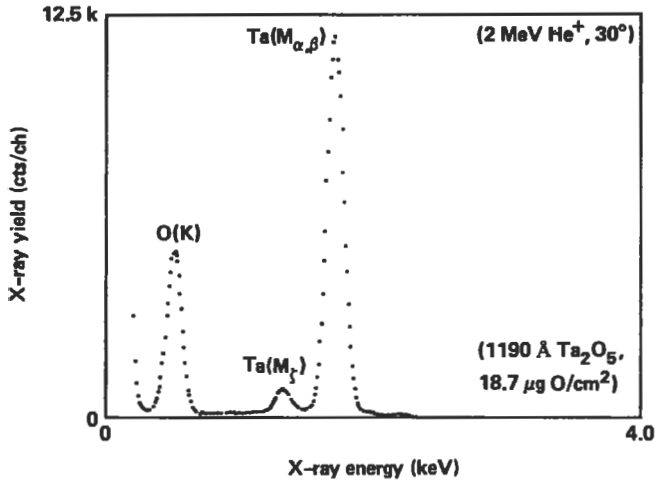

Figure 5 **Helium-ion induced X-ray spectrum from anodized tantalum (fluence = 1.5×10^{15} He^+/cm^2).[12]**

Depth Profiling of Surface Layers on Specimens

Rutherford Backscattering (RBS) provides quantitative, nondestructive elemental depth profiles with depth resolutions sufficient to satisfy many requirements; however, it is generally restricted to the analysis of elements heavier than those in the substrate. The major reason for considering depth profiling using PIXE is to remove this restrictive condition and provide quantitative, nondestructive depth profiles for all elements yielding detectable characteristic X rays (i.e., $Z > 5$ for Si(Li) detectors).

Because a PIXE spectrum represents the integral of all the X rays created along the particle's path, a single PIXE measurement does not provide any depth profile information. All attempts to obtain general depth profiles using PIXE have involved multiple measurements that varied either the beam energy or the angle between the beam and the target, and have compared the results to those calculated for assumed elemental distributions. Profiles measured in a few special cases suggest that the depth resolution by nondestructive PIXE is only about 100 nm and that the absolute concentration values can have errors of 10–50%.

Although depth profiling using nondestructive PIXE does not appear promising, PIXE in combination with RBS or with low-energy ion sputtering offers the possibility of quantitative depth profiles for elements with $Z > 5$. Because X rays and backscattered particles emanate from the specimen during ion irradiation, both should be detected. In fact, simultaneously performing PIXE and RBS eliminates ambiguities in the interpretation and modeling of the RBS results.[12] As an example, consider RBS results from high-Z materials with surface layers containing low-Z elements. In such cases, the RBS spectra are dominated by scattering from the high-

Z elements, with some indication of compositional changes with depth; PIXE provides unequivocal identification of the elements present and, with appropriate calibrations, the absolute areal densities of these elements.

Although not commonly available, the combination of PIXE and low-energy ion sputtering can provide quantitative, destructive depth profiles. PIXE measurements taken after each sputtering period give the quantity of each element remaining and, by difference, the number of atoms (of each element) removed during the sputtering period. Consequently, this combination can yield both the elemental concentrations and the conversion of the sputtering time or fluence to a depth scale. The achievable depth resolution would be determined ultimately by the precision of the PIXE results or nonuniform sputtering effects and could be about 1 nm at the surfaces of specimens.

Other Modes of Analysis

For the preceding modes, the discussion implicitly assumed the "normal" conditions for PIXE analysis (i.e., few mm-diameter beam, approximately constant beam current, and specimen in vacuum), and ignored the crystallographic nature of the specimen. However, some of the most interesting PIXE results have been obtained using other modes.

Reducing the ion beam to a small spot (1–10 μm) and scanning this microbeam across the specimen yields lateral concentration maps analogous to those obtainable with an electron microprobe, but with the advantages inherent in particle-induced spectra and with the potential of much higher spatial resolution, because the particle beam spot and the X-ray source volume have essentially the same lateral dimensions due to the nearly straight-line trajectory of the particles over their X-ray producing range.

External-beam PIXE refers to measurements with the specimen removed from a vacuum environment. This mode permits the analysis of large or volatile specimens and consists of allowing the particle beam to exit, through a thin window, the vacuum of the beam line and impinge on the specimen held at atmospheric pressure of air or other gases (e.g., helium).

The combination of PIXE with channeling of ions through the open directions (i.e., axial or planar channels) of monocrystalline materials can be used to determine the location of impurity atoms in either interstitial or substitutional sites or to assess the extent of lattice imperfections in the near-surface region. Channeling measurements are usually performed with RBS, but PIXE offers distinct advantages over RBS. First, because the PIXE cross sections are larger, the measurements can be performed with lower beam intensities or fluences. In addition, PIXE can be used to locate light elements in a matrix of heavy elements.

On-demand beam pulsing has been shown to be effective for eliminating pulse pileup in the X-ray detection system, minimizing the energy dissipated in delicate specimens, yet maximizing the data throughput of the overall system. In essence,

the on-demand pulsing system consists of deflecting the beam off the specimen when the detector's amplifying system begins to process a pulse and returning the beam to the specimen at the end of the pulse-processing time.[13]

Quantification

Quantification of raw PIXE spectra involves identifying all the peaks, determining the net counts under each peak, and correcting for the energy-dependence of the ionization cross sections as a function of depth in the material; the absorption of the X rays in the material; the production of secondary fluorescence; and the fraction of the X rays detected. In general, high accuracy in PIXE is achieved only for thin or homogeneous, thick specimens. Although PIXE spectra are routinely analyzed using least-squares fitting codes, the accuracies are ultimately limited by the accuracies of the fundamental data bases for ionization cross sections, fluorescence yields, ion stopping cross sections, and X-ray absorption effects, and by the calibration procedures used to determine the energy dependence of the fraction of the X rays detected.

A detailed comparison of the analysis of the same set of PIXE data using five different spectral fitting programs yielded remarkably good agreement for the results obtained.[14] The five least-squares fitting codes were used on PIXE spectra from a set of thin biological, environmental, and geological specimens. The results were the same within 5%, which suggests that PIXE analysis has matured to quite an acceptable level.

Similar accuracies have been found for thick, homogeneous, complex specimens when corrections for secondary excitation are also included. With appropriate standards, total accuracies of 2% have been demonstrated. Because the determination of the lighter elements (i.e., $5 < Z < 15$) are more sensitive to the uncertainties in the data base items listed above, less accuracy should be expected for these elements.

Artifacts

The major artifacts contributing to uncertainties in PIXE results stem from effects caused by bombardment of nonideal specimens, particularly thick specimens. The ideal thick specimen would be a homogeneous, smooth electrical conductor that does not change during bombardment. Except for rather simple, well-defined layered structures (e.g., surface oxide layers), specimens having compositional variations with depth yield spectra whose analyses can have large inaccuracies.

Changes in the composition of a specimen over the analyzed depth can be caused by beam heating or by beam charging of the specimen. Beam heating can lead to selective vaporization of some elements or diffusional redistribution of the elements. If the surface charges up to some potential, then electric-field enhanced diffusion can selectively redistribute certain elements. Beam-heating effects usually

can be mitigated by lowering beam intensities or by cooling the specimen. Electric-field enhanced diffusion can be controlled using the procedures described below for eliminating specimen charging by the beam.

Ion bombardment of electrically insulating specimens can lead to a surface charge giving a potential at the beam spot that can be significant (e.g., from a few kV to > 10 kV). Such potentials can cause surface discharges between the spot and the closest grounded conductor. The PIXE spectra would then contain characteristic and bremsstrahlung X rays excited by electrons participating in the discharges. Thus, the accuracy for the characteristic peaks would be reduced, and the relatively large bremsstrahlung radiation would hide the characteristic X-ray peaks of some trace elements. In addition, surface charging precludes accurate current integration from the specimen current, even when electron suppression is used. Standard procedures to eliminate or minimize these effects include neutralizing the surface with electrons from a hot filament or a thin metal or carbon foil placed in front of the specimen, but out of view of the X-ray detector; coating the specimen with a thin, conducting layer that either covers the bombarded spot or encircles the spot and leads to a conductor; and introducing a partial pressure of a gas (e.g., helium) into the chamber and letting ionization of the gas by the beam provide a conducting path to discharge the specimen.

The geometrical arrangement of the beam axis, the specimen normal, and the detection angle must be well known to obtain accurate PIXE results. A rough surface affects both the ion range and the X-ray absorption. The impact on accuracy will depend on the element of interest and the matrix. The largest effects occur for situations involving high X-ray absorption coefficients. As an example, yield variations of about 25% for sulfur in iron have been calculated for 10-μm grooves, when the groove direction is perpendicular to the detector axis.[15] Of course, minimal effects are expected when the detector views the specimen along the grooves.

Conclusions

Within the last 5–10 years PIXE, using protons and helium ions, has matured into a well-developed analysis technique with a variety of modes of operation. PIXE can provide quantitative, nondestructive, and fast analysis of essentially all elements. It is an ideal complement to other techniques (e.g., Rutherford backscattering) that are based on the spectroscopy of particles emitted during the interaction of MeV ion beams with the surface regions of materials, because

1. X rays also are emitted from the bombarded specimen.
2. Characteristic X rays provide an unambiguous identification of the elements present.
3. Quantitative analysis of low-Z elements on or in high-Z materials can be performed.

PIXE detection limits for surface layers on bulk specimens are sufficiently low to permit calibration of true surface analysis techniques (e.g., Auger electron spectroscopy).

Development of several existing trends can be expected to enhance the value of PIXE in the future. Analyses for low-Z elements (e.g., $5 < Z < 15$) should receive increased attention because of the availability of Si(Li) detectors with windows that transmit a large fraction of < 1-keV X, rays yet support atmospheric pressure. Appropriate modifications to the existing spectral fitting programs will be required to make quantification for low-Z elements a routine procedure. Since micro-PIXE equipment has just recently become available commercially, a proliferation of micro-PIXE capabilities can be anticipated. The demonstrated compatibility and usefulness of simultaneous PIXE and RBS should lead to routine applications of such measurements. With specific regard to surface analysis, arrangements combining PIXE with low-energy sputtering will allow quantitative, high-resolution depth profiling of materials. In addition, combinations of PIXE with true surface analysis techniques (e.g., AES and XPS) will improve greatly the quantitative accuracy of these techniques.

This work was performed under the auspices of the US DOE by Lawrence Livermore National Laboratory under contract no. W-7405-Eng-48.

Related Articles in the Encyclopedia

RBS, ERS, XRF, EDS, and EPMA

References

1 T. A. Cahill and J. Miranda, private communication, 1991.

2 S. A. E. Johansson and J. L. Campbell. *PIXE: A Novel Technique for Elemental Analysis.* John Wiley, Chichester, 1988. A detailed introduction to PIXE and the relevant literature.

3 J. P. Willis. *Nucl. Instr. Meth. Phys. Res.* **B35,** 378, 1988. A critical comparison of PIXE with XRF.

4 J. F. Ziegler, J. P. Biersack, and U. Littmark. *The Stopping and Range of Ions in Solids.* Pergamon Press, New York, 1985. Source book for TRIM calculations.

5 W. Brandt and G. Lapicki. *Phys. Rev.* **A20,** 465, 1979; **A23,** 1717, 1981. Original papers on ECPSSR calculations of cross sections.

6 D. D. Cohen and M. Harrigan. *Atomic Data and Nuclear Data Tables.* **33,** 255, 1985. Tabulated ECPSSR cross sections for protons and He^+.

7 F. Folkmann, C. Gaarde, T. Huus, and K. Kemp. *Nucl. Instr. Meth.* **116,** 487, 1974. First theoretical estimates of background in PIXE.

8 F. Folkmann. In: *Ion Beam Surface Layer Analysis.*(O. Meyer, G. Linker, and O. Keppeler, eds.) Plenum, New York, 1976, pgs. 695 and 747. Early experimental evaluation of X-ray background in PIXE.

9 R. G. Musket.In: *Advances in X-Ray Analysis.* (G.J. McCarthy et al., eds.) Plenum Publishing, 1979, volume 22, p.401. PIXE of C on and in Fe.

10 R. G. Musket. *Nucl. Instr.Meth. Phys. Res.* **B24/25,** 698, 1987. PIXE of O on and in Be.

11 J. L. Campbell and J. A. Cookson. *Nucl. Instr. Meth. Phys. Res.* **B3,** 185, 1984. A review of thick-target PIXE.

12 R. G. Musket. *Nucl. Instr. Meth. Phys. Res.* **218,** 420, 1983. Examples of simultaneous PIXE and RBS.

13 X. Zeng and X. Li. *Nucl. Instr. Meth. Phys. Res.* **B22,** 99, 1987. Details of fast, transistorized on-demand beam for PIXE.

14 J. L. Campbell, W. Maenhaut, E. Bombelka, E. Clayton, K. Malmqvist, J. A. Maxwell, J. Pallon, and J. Vandenhaute. *Nucl. Instr. Meth. Phys. Res.* **B14,** 204, 1986. Comparison of five PIXE spectral processing techniques.

15 J. A. Cookson and J. L. Campbell. *Nucl. Instr. Meth. Phys. Res.* **216,** 489, 1983. Calculated effects of surface roughness on thick-target PIXE.